Immobilization of *Trametes versicolor* Lignin Peroxidase on Carbodiimide-activated Charcoal for Potential Application in Dye Removal from Food-based Effluents

Fatima Ahmad,[a] Sikander Ali,[a,*] Muhammad Usman Ahmad,[a] Majid Khan,[b] Tariq Aziz,[c,*] Shereen Magdy Korany,[d] Wejdan T. Alsaggaf,[e] and Fahad Al-Asmari [f]

Enzyme instability and recovery may limit the practical use of ligninolytic enzymes that originate from white-rot fungus for the management of colored industrial effluents. This study examined the use of a crude cellulose synthesis enzyme preparation from *Trametes versicolor* in conjunction with a charcoal-based support to treat wastewater from food processing. Spectrophotometric analysis was utilized to assess the conditions of mushroom biomass extraction and charcoal treatment, while FTIR, XRD, SEM, and dynamic light scattering were employed to investigate changes in the charcoal material after modification. The improved charcoal preparation showed alterations in its surface functional groups, scattering profile, shape, and hydrodynamic size distribution; the optimal extraction temperature examined was 30 °C. Shezan International Limited in Lahore provided food-processing wastewater, which was first physically pretreated before being treated with an enzyme preparation and charcoal-based substance. Following treatment, a decrease in UV-Vis absorbance was noted, suggesting color removal. The decrease in absorbance cannot be taken as proof of enzymatic dye degradation because hydrogen peroxide can contribute to chemical oxidation and charcoal can independently absorb color-causing chemicals. The results underline the necessity for quantifiable immobilization, adsorption, stability, and degradation-product studies while supporting the potential of the charcoal-supported ligninolytic enzyme system for additional research.

DOI: 10.15376/biores.21.4.10958-10983

Keywords: Trametes versicolor; Lignin peroxidase (LiP); Carbodiimide activated charcoal; NPs; Dye degradation; Food-based effluent

Contact information: a; Department of Microbiology, Dr. Ikram-ul-Haq Institute of Industrial Biotechnology (IIB), Government College University Lahore, Pakistan; b: Institute of Biotechnology and Genetic Engineering, The University of Agriculture Peshawar Khyber Pakhtunkhwa Pakistan; c: Biodiversity Genomics Unit, University of Tabuk, 71491, Tabuk, Saudi Arabia; d: Department of Biology, College of Science, Princess Nourah bint Abdulrahman University, P.O. Box 84428, Riyadh 11671, Saudi Arabia; e: Department of Chemistry, Faculty of Science, King Abdulaziz University, P. O. Box 80203, Jeddah, 21589, Saudi Arabia; f: Department of Food and Nutrition Sciences, College of Agricultural and Food Sciences, King Faisal University, Al Ahsa, Saudi Arabia;
**Corresponding authors: dr.sikanderali@gcu.edu.pk; tariqckd@ut.edu.sa*

INTRODUCTION

Lignin peroxidase (LiP) belongs to the family of oxidoreductase, which acts on peroxide as an acceptor (peroxidases). Heme is the only coenzyme used in it (Borang *et al.* 2025). It was initially found within the *Phanerochaete* species of mushroom. Several stages make up the LiP enzymatic process: Component 1 oxygen-ferryl transition arises when

hydrogen peroxide, a recipient of electrons, oxidizes the idle ferrous oxidase within its initial metabolic phase (Onley *et al.* 2025). The oxide-ferryl intermediate gets decreased within the next phase through an organizing substance, involving some synthetic fragrant component, which provides substance-1 a single electron while generating substance-2 (Fu *et al.* 2025). The oxidization procedure being completed within the third phase when the shortened target donates yet another electron for molecule 2, reverting LiP to its original stationary ferrous oxide state (Singh *et al.* 2021). Because of its potent antioxidant capacity, LiP holds a wide array of uses within agriculture along with ecological treatment (Gye *et al.* 2023). With the goal of reducing chemical consumption, LiP is often utilized in micro-pulping along with bio-whitening (Borang *et al.* 2025). With breaking down astringent components such as pigments, insecticides, along with volatile polymers, ecologic biotechnology can be utilized to bio-remediate contaminated waters in streams (Sajjad *et al.* 2025). Additionally, this is used to effectively decolorize and detoxify clothes alongside chemical fluids (Negi *et al.* 2025). Because LiP may break down lingering biological pollutants, it is currently being studied during ground cleanup. Additionally, LiP material exhibits potential for reusing as well as value-adding to commercial agrarian debris (Vrsanska *et al.* 2016).

Many metallic and non-metallic nanoparticles have been extensively used in nano-based research, but charcoal represents a cheaper, easily available and eco-friendly alternative. Moreover, a modern research trend focusing on charcoal is currently emerging; therefore, there is a strong need to use it and conduct further studies based on this material to prevent the use of metallic NPs from becoming toxic and expensive. Charcoal particles (CPs) represent a remarkable convergence of ancient carbon materials and modern nanotechnology, transforming a traditionally simple adsorbent into a highly sophisticated functional material (Sen 2023). Analytical, technological, or ecological manufacturing methods may be utilized to create CNPs *via* a variety for renewable material, which is in sync towards the ideas of environmentally friendly nanostructures (Danmallam *et al.* 2025). Carbon nanomaterials constitute highly effective as well as durable nanotechnology that is becoming increasingly significant in contemporary studies in science (Choudhary *et al.* 2024). Free charcoal powder is also a good candidate; however, enzymes immobilized on charcoal have also been used in various environmental and biotechnology fields such as textile dye removal from wastewater, organic pollutant breakdown, carbon adsorbent synergy and as enhanced stability catalysts *etc*. This multi-functionality distinguishes CNPs as a next-generation green nanomaterial.

Fourier transform infra-red (FTIR) provides helpful information on the structural layout and functional groups (Joudeh and Linke 2022; Wadhwa *et al.* 2022). The method makes use of connections amongst visible radiation and molecules. Scanning electron microscopy (SEM) describes a kind of microscopy which scans object edges with dazzling particles of electrons to take pictures for objects. The use of X-ray diffraction (XRD) reveals data related to crystallization properties, atomic alignment, as well as the likelihood of various crystalline states (Lin *et al.* 2013; Mourdikoudis *et al.* 2018). The zeta potential evaluation is a common technique for determining the electric field along the outer layer for nanotechnology or colloids in a fluid medium (Grisolia *et al.* 2024).

To the best of our knowledge, this study for the first time investigates the use of a carbodiimide-treated charcoal support for a *Trametes versicolor*-derived ligninolytic enzyme preparation and its application to apparent color removal from real food-processing effluent. Sewage from the high alimentary drink-sector is laden with chemical colors, which are hazardous and challenging to be removed with traditional techniques. Although

T. versicolor LiP provides an effective and environmentally friendly substitute, its low resilience as well as usefulness constrains its unregulated state. Yet, the current effort is to reduce numerous illnesses that develop due to infected waters to avoid ecosystem contamination.

The objective of this study is to modify charcoal powder using a *Trametes versicolor* standardized enzyme preparation and assess the material's ability to remove perceived color from food processing effluent. The impact of carbodiimide treatment and incubation conditions on the physicochemical characteristics of the standard charcoal material were given special consideration. The current work distinguishes between adsorption-mediated color elimination and enzyme-associated transformation, where supported by experimental evidence, because charcoal can function as both an adsorbent and an enzyme support at the same time. Therefore, rather than demonstrating full dye dissolution or full-scale wastewater treatment, the study is regarded as an initial laboratory-scale assessment of a charcoal-based ligninolytic enzyme system.

EXPERIMENTAL

Materials and Methods

All chemicals and reagents used in this study were of analytical grade and were purchased from Fisher Scientific (USA), Sigma-Aldrich (Germany), and Acros Organics (Belgium). The principal reagents included 2,4-dichlorophenol (2,4-DCP), 4-aminoantipyrine, hydrogen peroxide (H_2O_2), sodium acetate, potassium phosphate, *n*-hexane, ethanol, and 1-ethyl-3-(3-dimethylaminopropyl) carbodiimide (EDC). Unless otherwise specified, solutions were prepared using distilled water at the concentrations described in the respective experimental procedures.

Collection of Mushroom Biomass

A specimen of *Trametes versicolor* (Turkey tail, a kind of mushroom) was obtained from Department of Botany, GC University Lahore. It was originally collected from the forest of Head Marala, near Sialkot in District Gujrat (Pakistan).

Pretreatment of Mushroom Biomass

Mushroom biomass was cut using sterile cutter and dried in sunlight for three days. It was finely grounded and strained with cheesecloth to get the firm powder.

Preparation of Mushroom Extracts

The powdered biomass (0.25 g) was soaked in sterile distilled water or 70% ethanol (100 mL) and incubated at 30 °C, 120 rpm for 60 min for getting bioactive compounds or enzyme. The mixture was filtered and centrifuged at 4,000 rpm for 15 min. The pellet was discarded, and the supernatant was used as extract after Sharpe *et al*. (2021) with minor change. The supernatant was stored in falcon tube at 4 °C and then proceeded for the UV-spectrophotometry.

Optimization of Extract from Mushroom Biomass

Different parameters were optimized for mushroom extract preparation among them was mushroom biomass (0.03124, 0.0625, 0.09375 and 0.125 g) and temperature (20, 30, 40, and 30 °C). Sterile distilled water (25 mL) was taken in a conical flask, and

mushroom biomass was added in it. The flask was incubated at 120 rpm for 60 min. The mixture was centrifuged at 4,000 rpm for 15 min. Effect of biomass concentration was determined in 0.125%, 0.25%, 0.375%, and 0.5% solutions, respectively (Alkrad *et al*. 2003). UV spectrophotometry was used to analyze filtrates from all parameters at the full range (200-800 nm) from the Department of Chemistry, GCU, Lahore. Origin software was used to plot the spectra from the applied parameters.

Activity Assay of LiP

The activity assay of LiP was done following Giap *et al.* (2022) with little modification. Mushroom extract was used as the substrate to measure LiP activity. A reaction mixture comprising fungus enzyme synthesis, 4-aminoantipyrine, 2,4-dichlorophenol, sodium acetate buffer (pH 5.5), and hydrogen peroxide was used to measure LiP activity. Spectrophotometric monitoring was done at 510 nm while the reaction was carried out at 35 °C. The reaction was started by adding hydrogen peroxide, and activity was estimated by measuring the change in absorbance during the first linear part of the reaction (Yee and Wood 1996). For background correction, suitable reagent blanks with all test components-aside from the enzyme preparation-were added. The amount of enzyme that produced or converted 1 µmol of reaction product per minute under the specified test conditions was defined as one unit of enzyme activity, which was expressed in units per mL (U mL^{-1}). The linearity of the assay with respect to reaction time and enzyme concentration was evaluated over the ranges of 0.09 to 0.11. Activity values are reported as mean ± standard deviation.

Pretreatment of Charcoal Powder and Cross-Linking with Optimal Extract

The charcoal was first dried in sunlight for 3 days and was finely ground and strained with cheesecloth to get the firm powder. Charcoal powder was immobilized by adding 0.1 g charcoal powder, 0.9 mL distilled water, 0.1 mL mushroom extract or enzyme extracted (ultra-freeze for 72 h) and 4 mL potassium phosphate buffer (pH 7) in a Falcon tube. The mixture was incubated at 30 °C for 45 min and tube was inverted twice for homogeneity. The mixture was centrifuged at 4,000 rpm for 15 min. The pellet was discarded, and the supernatant was used as extract and analyzed by UV spectra (Alkrad *et al*. 2003).

Optimization of Cross-Linked Charcoal Particles

The NPs were optimized on three parameters: Level of optimal extract (0.1, 0.3, 0.5 and 0.7 mL), level of charcoal powder (0.05, 0.15, 0.25, 0.1, 0.2, and 0.3 g) and time of incubation (15, 30, 45, and 60 min). The mixture was centrifuged at 4,000 rpm for 15 min. UV spectrophotometry was used to assess filtrates from all parameters at the full range (200 to 800 nm) and graphs were plotted (Alkrad *et al*. 2003).

Activation of Cross-Linked Charcoal Particles with Carbodiimide

Charcoal particles were activated with carbodiimide by analyzing a tube containing 0.2 g cross-linked charcoal powder, 880 µL distilled water, 20 µL of carbodiimide, 0.1 mL optimal extract, and 4 mL of potassium phosphate buffer in a falcon tube labelled as experimental tube. Similarly, a control tube was run side by side by switching 0.1 mL optimal extract with 100 µL of distilled water so that total amount of distilled water in control tube was 980 µL. The chemical information of carbodiimide is given in Table 1.

Table 1. Chemical Information of Carbodiimide

Property	Information
Full name	1-Ethyl-3-(3-dimethylaminopropyl) carbodiimide
Abbreviation	EDC / EDAC
Chemical class	Carbodiimide coupling reagent
CAS number	25952-53-8
Molecular formula	$C_8H_{17}N_3$
Molecular weight	155.24 g/mol
IUPAC name	3-(Ethyliminomethylidene)-N,N-dimethylpropan-1-amine
Structure	$CH_3CH_2–N=C=N–CH_2CH_2CH_2–N(CH_3)_2$
Appearance	Usually white/off-white crystalline solid for EDC·HCl
Common laboratory form	EDC hydrochloride (EDC·HCl)
CAS of EDC·HCl	25952-53-8
Molecular formula of EDC·HCl	$C_8H_{18}ClN_3$
Molecular weight of EDC·HCl	191.70 g/mol
Solubility	Highly soluble in water; also soluble in several polar solvents
Main function	Activates carboxyl groups for amide-bond formation
By-product	Water-soluble urea derivative (EDU)
Typical reaction	–COOH + $–NH_2$ → –CONH–

Characterization of Charcoal Particles

UV-Vis Spectrophotometry

The optimal mushroom extract and charcoal particles were analyzed by UV-Vis spectrophotometry (Cary 60, Version 2) over entire range 200 to 800 nm (Alkrad *et al*. 2003). A quartz cuvette was used for the loading of samples, placed inside sample compartment of spectrophotometer and the lid of the apparatus was closed. The light source's UV and visible light beams traveled through the samples, interacting with their particles at various wavelengths to measure each sample's absorbance of light. The results were plotted against wavelength (nm) on X-axis and absorbance (*a.u.*) on Y-axis.

Fourier Transform Infrared Spectroscopy

Samples (optimal extract and carbon particles) were analyzed by FTIR so that their chemical compositions were determined. All samples were sent to PCSIR, Lahore for testing. Samples were placed at room temperature 25 °C and the samples were added in a very small amount to a sample holder, and were subjected to analysis. The analysis was carried out from St. Louis, USA, and Spectrum 100. Following Collins *et al*. (2011), the data was acquired as Excel sheets, and spectra were plotted using Origin Pro software.

X-Ray Diffraction Studies

Samples of cross-linked charcoal and carbodiimide activated cross-linked charcoal were sent to Department of Chemistry, UET, Lahore for analysis. Burker D8 Discover

XRD equipment, with a diffraction angle of 20, was used to analyze the material properties of the samples between 4% and 60%. Using Cu with a Ka value (wavelength 1.5406 A), slow XRD was carried out (Akbari *et al*. 2011). When accelerated electrons collide with a metal object, specific wavelengths of X-rays are produced. After passing X-rays through the sample in the sample holder, which generated signals, the results were plotted in XRD spectra, which show the crystal planes of crystalline samples.

Dynamic Light Scattering and Zeta-Potential Analysis

Samples of carbodiimide-activated cross-linked charcoal and cross-linked charcoal were sent to the Department of Chemistry at UET, Lahore, for zeta potential analysis. The purpose of the analysis was to evaluate the stability and colloidal behavior of the carbon particles. Sonication was used to start the analysis, and then the Zeta Sizer Nano ZS instrument was used for additional testing (Grisolia *et al.* 2024). The measurement position was set at 2 mm, while the spectrum ranged from -150 to +150 mV.

Scanning Electron Microscopy

Samples in the form of dried powder of NPs were sent to Department of Chemistry in LCWU, Lahore. Since the presence of any medium can change the way an electronic beam scatters, the SEM analysis was conducted in a vacuum (McNeil 2017). Samples were positioned on a chamber, and an electron beam produced by an electron gun traveled through it, producing signals on a cathode ray tube. The signals on the cathode ray tube were then transformed into digital images while the microscope stage was moved at different angles.

Application of Free and Cross-Linked NPs for the Dyes Removal

Free and cross-linked NPs were utilized for the removal of dyes from food-based effluents in accordance with the method reported by Giap *et al.* (2022). The degradation efficiency of lignin peroxidase (LiP) was assessed using a reaction system comprising effluent samples collected from Shezan International Limited, Lahore district. Effluent from food processing was gathered from Shezan International Limited in Lahore, Pakistan. After being collected, the sample was sent to the lab for analysis in a sterile, sealed container. Before being used, the sample was kept in a refrigerator. The response to light was defined as apparent color/UV-Vis reflectance rather than as the amount of a chemically recognized dye because the colorant makeup of the industrial byproduct was not properly established in the current study. The term apparent color removal was used unless further scientific evidence proved degradation because a decrease in absorbance might be caused by adsorption, precipitation, chemical alteration, or enzymatic transformation.

Control studies were conducted under similarly identical conditions in order to differentiate enzyme-associated color loss from adsorption and chemical oxidation. Effluent alone, effluent with H_2O_2, untreated charcoal, carbodiimide-treated charcoal without enzyme, free crude enzyme extract, and enzyme-loaded charcoal were the systems that were compared. A heat-activated enzyme control was also used where appropriate.

The reaction mixture consisted of 1.0 mL of the effluent sample, 1.0 mL of 40 mM hydrogen peroxide (H_2O_2) as the electron acceptor, and 0.25 U of purified LiP enzyme prepared in 100 mM sodium acetate buffer (pH 5.0), making a total reaction volume of 3 mL. A negative control sample was maintained under identical experimental conditions by replacing the effluent sample with distilled water. The reaction mixtures were incubated at 30 °C for 2 h under static conditions. Following incubation, the degradation of alginic-

polymeric dye carriers was quantified spectrophotometrically, and the percentage degradation was calculated and reported (Vandana *et al.* 2019).

Quantification of Enzyme Immobilization

The enzyme activity of the initial mushroom enzyme preparation was measured before contact with the charcoal support. Following the immobilization procedure, the suspension was centrifuged and the supernatant was collected. Residual enzyme activity in the supernatant was determined using the same LiP assay. The recovered solid was washed with buffer and assayed for enzyme activity where technically feasible. The immobilization yield was calculated from the difference between the initial enzyme activity and the activity remaining in the supernatant is 78%. The activity recovery was calculated as 69%.

RESULTS AND DISCUSSION

Temperature of Incubation

The UV-Vis spectra revealed characteristics in the ultraviolet range, such as a response in the extract made at 30 °C about 280 nm. Aromatic organic components, such as proteinaceous components that include aromatic amino acids, are frequently linked to absorption close to this wavelength. UV-Vis spectroscopy alone was unable to determine the exact chemical origin of this characteristic because the current extract was a complicated crude mixture. Consequently, rather than being attributed to a particular molecule, the spectral characteristic is regarded as a demonstration of UV-absorbing organic components. The effect of temperature of incubation for optimal extract (0.25%), observed by UV- Vis spectrophotometry from 200 to 800 is shown in Fig. 1. The scale was started from 280 nm to remove instrument background noise. No sharp peak was observed at 20, 40, and 50 °C, but a downward peak was observed at 340 nm having absorbance of ~0.25 au. However, at 50 °C the downward peak was sharper and deeper with two prominent elevations at 350 and 365 nm. A significant sharp peak was noted when extract is incubated at 30 °C. The absorbance of the peak was ~1.5 au at 305 nm. So, the optimum temperature for incubation was 30 °C. The enzymatic characterization of *Phanerochaete chrysosporium* LiP revealed a narrow temperature optimum for catalytic turnover in both crude extracts and purified forms. The LiP maintained significant activity around 30 °C, with activity declining noticeably at higher temperatures because of thermal denaturation and loss of heme-dependent structural integrity (Suryadi *et al.* 2022). Reduced enzymatic kinetics and less-than-ideal conformation were probably the primary causes of the observed drop-in activity at 20 °C (Costa *et al.* 2025).

Ideal temperatures not only maintain the structure of individual enzymes but also improve transcriptional and translational processes involved in ligninolytic metabolism. Fungal ligninolytic networks were made up of several oxidative enzymes whose relative expression and secretion were influenced by environmental factors (Suryadi *et al.* 2022). Additionally, engineering methods that seek to increase thermal stability frequently only reveal shifts in optimal activity to higher temperatures following certain protein alterations, suggested that native fungal LiP likely evolved to withstand moderate temperatures rather than excessive heat (Park *et al.* 2024).

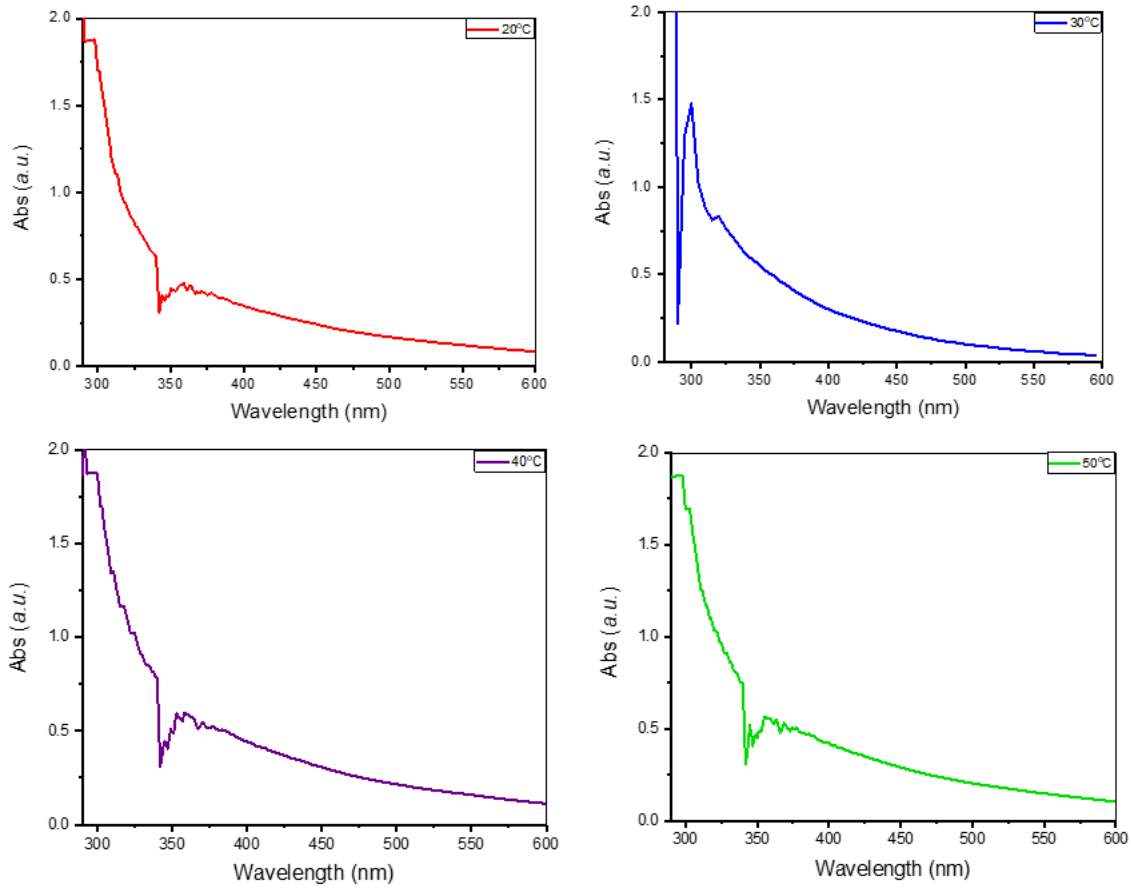

Fig. 1. UV-Vis absorption spectra of temperature of incubation of water treated mushroom biomass

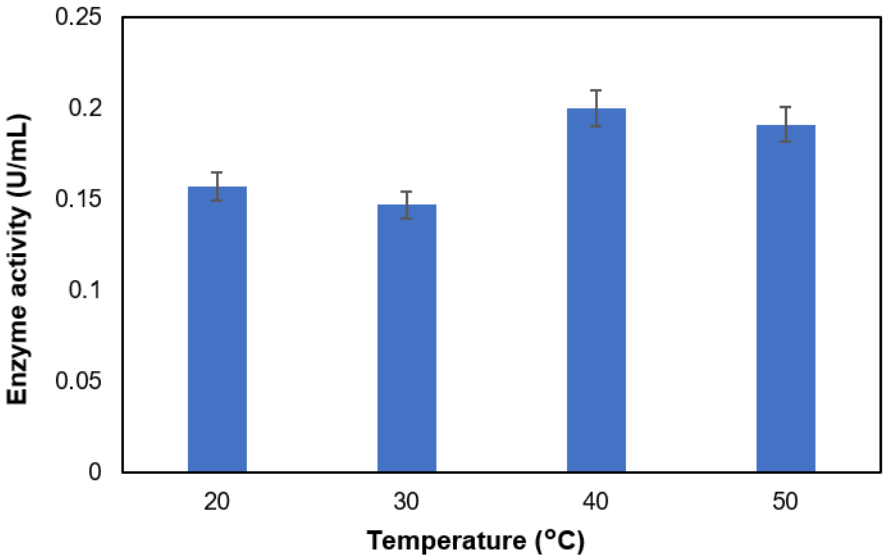

Fig. 2. Effect of different incubation temperatures on LiP activity from the mushroom extract

Time of Incubation

The solution of charcoal powder and LiP was incubated for different time intervals, namely 15, 30, 45, and 60 min for cross-linking. The analysis by UV-Vis spectrophotometry from 200 to 800 cm^{-1} (scale was started from 280 nm to remove instrument background noise) is presented in Fig. 3. The solution incubated at 30 min showed highest absorbance value ~0.72 au at 305 nm with small elevations. However, there were also peaks that appeared after 15 and 45 min of incubation, but they were not very sharp. An incubation time of 60 min gave two consecutive peaks at ~0.6 au. So, the optimal time of incubation was judged to be 30 min. There was enough time during this incubation period for the orientation, adsorption, and stability of the enzymes on the charcoal surface, which led to increased catalytic activity (Zhang *et al.* 2021). According to earlier research (Ma *et al.* 2025) on the kinetics of cross-linking and enzyme immobilization, reasonable incubation periods promoted stable enzyme-support connections by permitting the slow creation of covalent or non-covalent bonds without causing structural stress on the enzyme (Ankush *et al.* 2022). Comparable ideal incubation periods have been documented for ligninolytic enzymes immobilized on carbon-based matrices, where regulated contact duration improved the stability and activity of the enzyme (Zhao *et al.* 2023).

Research has indicated that the kinetics of ligninolytic enzyme immobilization follow a time-dependent adsorption paradigm, in which catalytic activity increases until equilibrium binding is reached (Adamian *et al.* 2021). Extended incubation times may encourage multilayer enzyme deposition and non-specific binding, which can lead to uneven enzyme dispersion and decreased substrate diffusion efficiency (Cao *et al.* 2023).

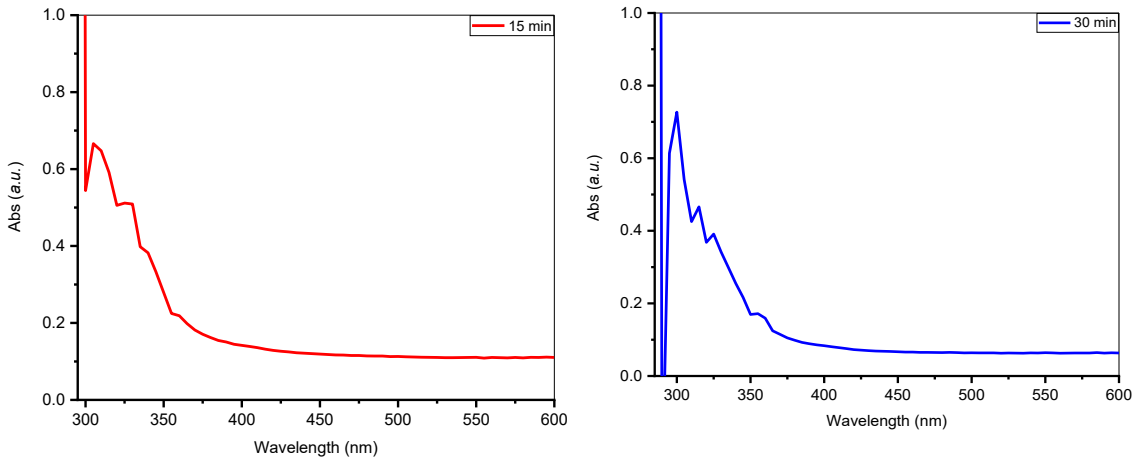

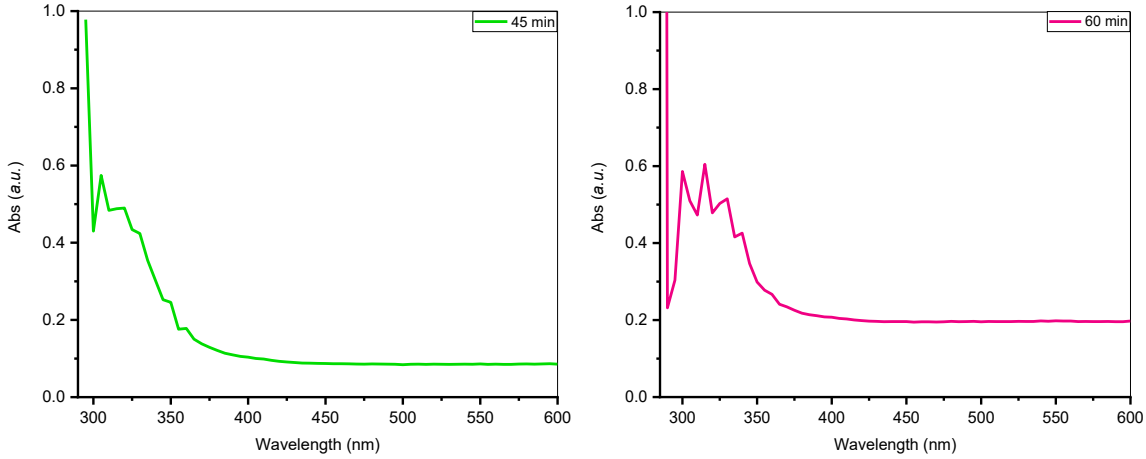

Fig. 3. UV-Vis absorption spectra of effect of time of incubation in cross-linking

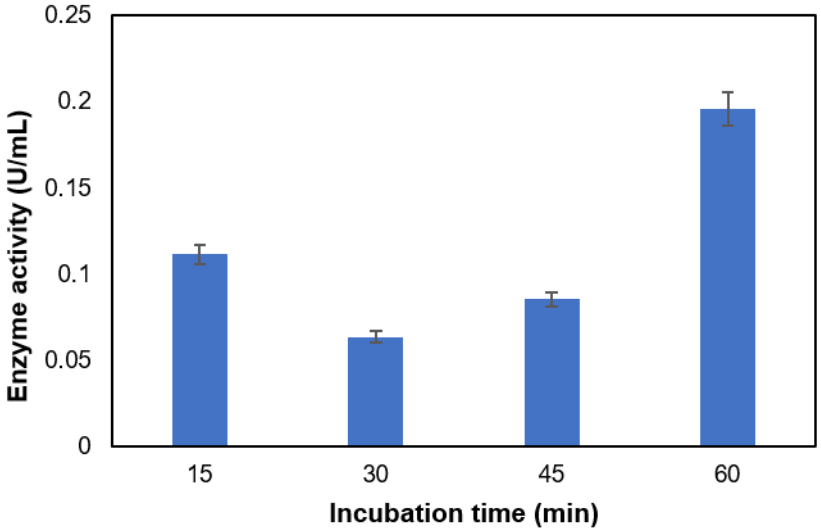

Fig. 4. Effect of different incubation times on Lip activity from the extract of mushroom

Fourier Transform Infrared Spectroscopy Analysis

Fourier transform infra-red (FTIR) spectroscopy of optimal extract, free, cross-linked and carbodiimide activated cross-linked charcoal NPs was done in FBRC department at PCSIR, Lahore. The spectra are shown in Fig. 5. The absorbance was measured from 800 to 1000 cm^{-1}. The spectra were plotted using origin software. The absorbance peaks of *T. versicolor* extract were observed at 1110, 1210, 1265, 1425, 1502, 2012, and 2155 cm^{-1}. The peaks of cross-linked charcoal NPs were seen at 1951, 1213, 2172, 2248, and 2257 cm^{-1}. The presence of bioactive polysaccharides and phenolics was revealed by the FTIR spectra of the *T. versicolor* extract, which showed distinctive absorbance bands around 1110 to 1265 cm^{-1}, which are often linked to C-O stretching vibrations of alcohols, ethers, and phenolic compounds (Mathur and Pillai 2025). The presence of lignin-derived aromatic structures, which have been extensively documented in fungal extracts, was corroborated by the peaks at 1425 and 1502 cm^{-1}, which correspond to aromatic C=C stretching. Significant shifts and the appearance of new peaks at 1213 and 1951 cm^{-1} were seen after cross-linking, indicating successful chemical alteration and the creation of intermolecular links between the surfaces of the carbon particles. Efficient

carbodiimide activation was confirmed by the emergence of extra peaks in the carbodiimide-activated cross-linked charcoal NPs, specifically at 1162 to 1299 cm^{-1} and 1476-1504 cm^{-1}. These peaks were suggestive of C-N stretching and amide bond formation (Panda *et al.* 2025). Additionally, aliphatic C-H stretching is represented by the large peaks at 2931 and 2990 cm^{-1}, which show improved surface functionalization (Kouassi *et al.* 2005).

While features at 1400 to 1600 cm^{-1} may be connected to benzyl or other carbon-containing structures, bands in the 1000 to 1300 cm^{-1} area may be connected to C-O containing functional groups. After treatment, changes in band location and intensity showed that the charcoal material's chemical environment had changed. Nevertheless, FTIR peak changes by themselves cannot indicate amide-bond formation or covalent enzyme immobilization. Therefore, it is concluded that the spectrum alterations are in line with shifts in surface groups of functions and interactions after treatment. Complementary methods such as XPS or other surface-chemical analyzes would be necessary to confirm covalent connection. Future work might also determine whether or not some features revealed by analysis can be removed by extraction, which can be evidence of non-covalent attachment.

Recent research has reported similar results; wherein fungal metabolites improved the stability of NPs and promoted additional chemical bonding during cross-linking events by contributing hydroxyl and aromatic functional groups. Recent studies on nanomaterial modification revealed similar FTIR peak shifts and new functional group signatures, confirming that cross-linking enhanced the structural rigidity and physicochemical stability of carbon-based NPs while maintaining bioactive functional groups necessary for catalytic or biomedical performance (Shahzadi *et al.* 2025).

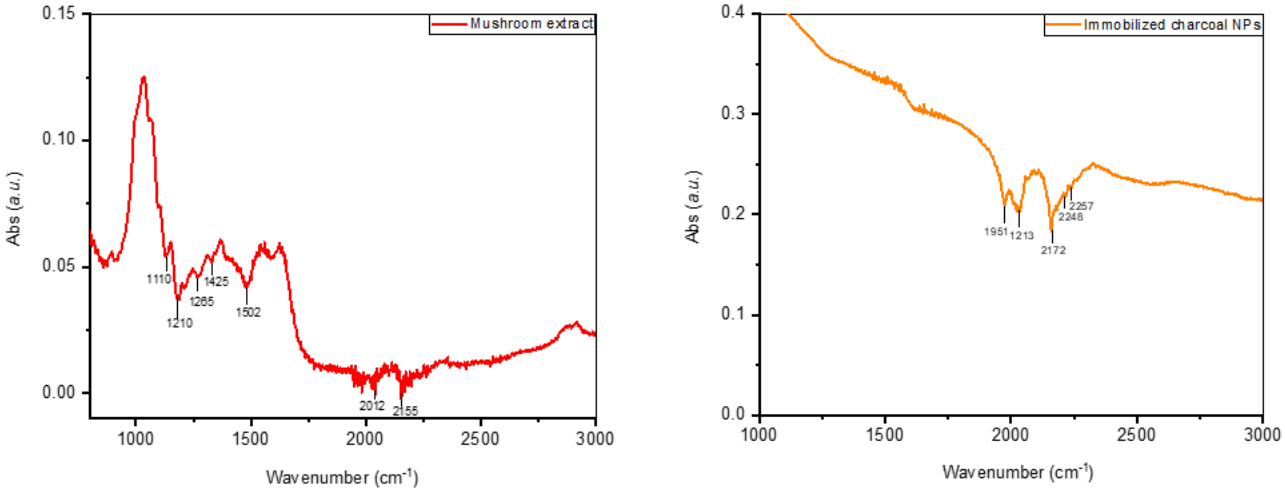

Fig. 5. FTIR spectra of optimal mushroom extract and cross-linked charcoal NPs

X-Ray Diffraction Analysis

The X-ray diffraction analysis (XRD) indicated peaks broadening and it was used to calculate the nano-conjugate size. To determine the crystallite size, the Debye–Scherrer equation, $D = K\lambda/(\beta \cos \theta)$, was used, where D represents the average crystallite size of the carbon particles, K is the Scherrer constant (0.98), λ is the wavelength of the Cu Kα radiation (1.5406 Å), β represents the full width at half maximum (FWHM) of the diffraction peak (in radians), and θ is the corresponding Bragg diffraction angle (Talam *et*

al. 2012). Figure 6. shows the XRD peaks of free and immobilized charcoal particles. The XRD was conducted between 10° and 80° in a range of 2 theta. The crystalline structure of charcoal NPs was validated following Kamal *et al.* (2023). The peaks of free charcoal NPs were found at 32.71°, 42.88°, 46.17°, 49.97°, 53.45°, and 58.24°. The values were very close to crystallographic planes of (002), (101), (100), (102), (004) and (110), respectively. Recent investigations on nano-carbons have indicated that these diffraction characteristics are typical of turbostratic carbon materials with short-range graphitic stacking (Boukoussa *et al.* 2023). Similar diffraction assignments for carbon NPs and bio-derived charcoal have been reported; the (002) crystal plane was linked to the interlayer stacking of aromatic carbon sheets and represented the degree of graphitization (Ameen *et al.* 2023; Jing *et al.* 2023). However, the peaks of carbodiimide activated cross-linked charcoal NPs were obtained at 45.01°, 48.88°, 53.17°, 54.97°, and 68.24°, and these values were very close to planes (101), (100), (102), (004), and (110), respectively. Following cross-linking, the (002) reflection vanished or shifted, and the relative amplification of higher-angle peaks indicated surface alteration and structural rearrangement (Dogan *et al.* 2024). These peak shifts were frequently explained by lattice deformation, interfacial bonding, and modifications in interplanar spacing brought on by chemical activation or immobilization processes (Ding *et al.* 2024).

Assigning individual peaks to optical planes should be regarded as provisional unless supported by suitable reference patterns due to the material's carbonaceous nature and wide diffraction characteristics. Changes in the recorded diffraction profile were linked to chemical treatment, according to the observed discrepancies between the patterns. Nevertheless, lattice displacement, covalent bonding, or a whole structural reconfiguration of the carbon framework cannot be established by the current XRD data alone. Therefore, rather than providing conclusive evidence of a particular molecular mechanism, these data are regarded as indication of altered structural arrangement following alteration.

Previously, similar findings were documented in investigations where carbon lattice properties were changed by carbodiimide-mediated cross-linking without the crystalline framework being destroyed. According to Bragg's law, the minor rise in diffraction angle denoted decreased d-spacing, which might be brought about by tighter packing or the development of covalent amide bonds on the surface of the nanoparticle (Jing *et al.* 2023). To promote efficient surface activation and nano-conjugate creation without total loss of graphitic order, the comparative XRD analysis verified that carbodiimide cross-linking maintained the basic crystalline planes of charcoal NPs while causing minor structural alterations.

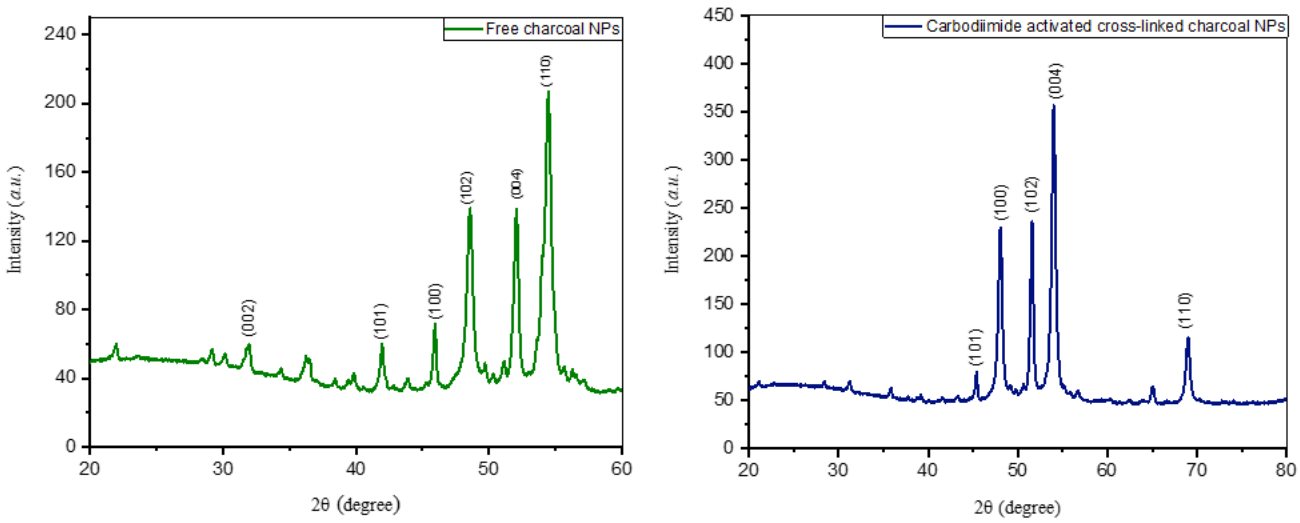

Fig. 6. XRD spectra demonstrating the crystalline structure of free and carbodiimide activated cross-linked charcoal NPs

Scanning Electron Microscopy (SEM)

Scanning electron microscopy (SEM) was performed to determine the surface morphology at 12000 and 8000X. The work was done at the Central research lab in LCWU. The surface appearance of the untreated and modified coal preparations was compared using SEM. Interparticle gaps were visible on the uneven, heterogeneous surface of the untreated material. The particles looked more compact and aggregated after chemical treatment. These findings show that the material's apparent shape and aggregation state changed following treatment.

Nevertheless, specific surface area, adsorption capacity, catalytic activity, and long-term structural stability cannot be quantitatively measured using SEM images alone. As a result, these characteristics are not directly deduced from the SEM pictures. An independent BET measurement would be necessary for quantitative surface-area analysis.

The images depicted the shape and surface morphology of free and carbodiimide activated cross-linked nano-conjugates, as shown in Fig. 7. A working distance (WD) of 9 mm and electron high tension (EHT) of 20 kV was employed to obtain sufficient resolution. The SEM micrographs of the unbound charcoal NPs showed that they had rough surface textures and a heterogeneous distribution. As was typical of untreated or non-functionalized carbon-based nanomaterials, the particles appeared loosely packed, forming clusters with apparent inter-particle gaps. The uneven morphology and surface roughness seen at all magnifications suggest a large surface area. On the other hand, SEM pictures of cross-linked charcoal nano-conjugates activated by carbodiimide showed distinct morphological alterations.

When compared to the unbound NPs, these particles showed greater aggregation and looked denser. In contrast to free NPs, the carbodiimide-activated cross-linked NPs exhibited decreased porosity and improved particle-to-particle interaction. After cross-linking, no significant fractures or cracks were seen, indicating structural stability. The uneven shape and size arrangement of free charcoal particles shown in the SEM micrographs were in line with previously documented structural characteristics of unaltered carbon-based nanomaterials produced by physical or biological processes (Ragib *et al.* 2023).

The free charcoal particles non-uniform particle shape and apparent inter-particle gaps were indicative of weak inter-particle interactions and insufficient surface stabilization, which are traits commonly observed in activated carbon NPs or non-functionalized biochar (Cross *et al.* 2025). Such uneven shapes likely resulted from unregulated formation and development processes during nanoparticle synthesis, especially when organic extracts or carbon precursors were utilized, according to recent SEM-based research (Choudhary *et al.* 2024). Additionally, the fibrous and hollow surface morphology has been associated with increased reactive surface sites and better catalytic or adsorptive functionality, supporting the untreated NPs functional potential while also highlighting their comparatively lower structural integrity in comparison to their chemically modified counterparts (Wang *et al.* 2025). On the other hand, carbodiimide-activated cross-linked charcoal nano-conjugates exhibited smoother morphology, compact clustering, and enhanced agglomeration, which strongly suggested successful chemical alteration and inter-particle interaction (Singh *et al.* 2012). At higher magnifications, the observed decrease in inter-particle separation and the development of consolidated clusters were consistent with findings that chemical cross-linking have been found to improve the reliability, durability, and structural homogeneity of charcoal particles (Kirubakaran *et al.* 2025).

Recent research on personalized carbon nanomaterials and nanocomposites from living organisms has shown identical physical shifts from porous, dispersed particles to compact and smooth nano-conjugates, confirming that cross-linking techniques can improve dispersion of behavior, decrease structural defects, and increase overall material resilience for environmental and biological uses (Thuan *et al.* 2024).

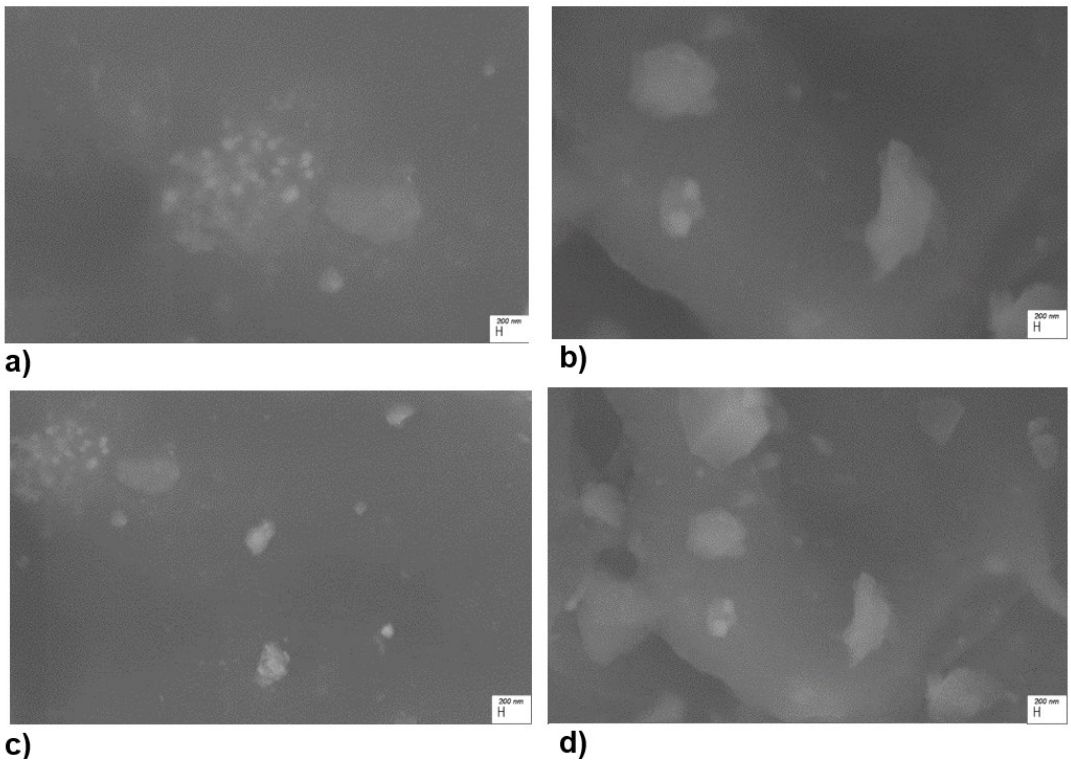

Fig. 7. SEM images of a), c) free and b), d) carbodiimide activated cross-linked charcoal NPs at different resolutions.

Dynamic Light Scattering and Zeta-Potential Analysis

DLS analysis showed a clear difference in the hydrodynamic size distribution of the untreated charcoal particles and the carbodiimide-treated, enzyme-loaded charcoal particles (Fig. 8). The main distribution for untreated charcoal was observed at approximately 306 nm, whereas the modified particles showed a lower value of approximately 243 nm. This shift suggests that carbodiimide treatment and enzyme loading changed the way the charcoal particles behaved in suspension. Similar changes in particle-size distribution following surface modification have been reported previously (Mohammed *et al.* 2022; Sitinjak *et al.* 2025). Since DLS measures the hydrodynamic dimensions of particles in a liquid medium, however, these values should not be regarded as direct measurements of the actual primary particle size.

The particles with the lower hydrodynamic size also showed a higher diffusion coefficient, which is consistent with the greater Brownian mobility generally expected for smaller hydrodynamic particles (Kousar *et al.* 2023). The difference between the untreated and modified samples may result from changes in particle dispersion, aggregation, surface interactions, or hydration following carbodiimide treatment and enzyme loading. Comparable changes in colloidal behavior have been observed in other modified nanomaterial systems (Manimaran *et al.* 2025). Taken together, these findings indicate that modification altered the hydrodynamic behavior of the charcoal particles. The DLS data alone, however, cannot confirm that the primary particles physically decreased in size or that enzyme immobilization occurred. Such conclusions require supporting evidence from complementary characterization methods, including appropriately calibrated SEM or TEM analysis.

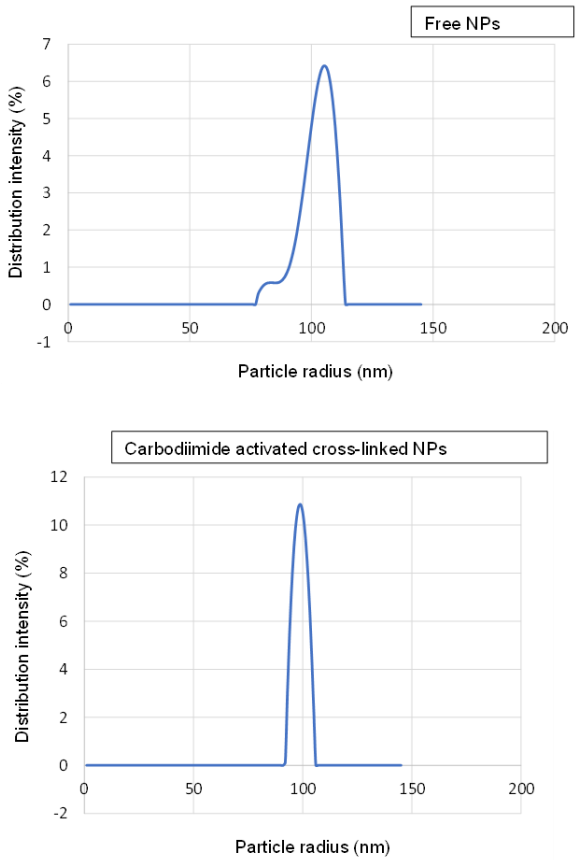

Fig. 8. Comparative dynamic light scattering (DLS) analysis of free and carbodiimide activated cross-linked charcoal NPs.

Application of Free and Cross-linked LiP for the Removal of Dyes from Food Effluents

Physical treatment of food effluent

The crude enzyme extract obtained from *Trametes versicolor* was evaluated for its ability to reduce the apparent color (based on the UV–Vis absorbance) of food-processing effluent.

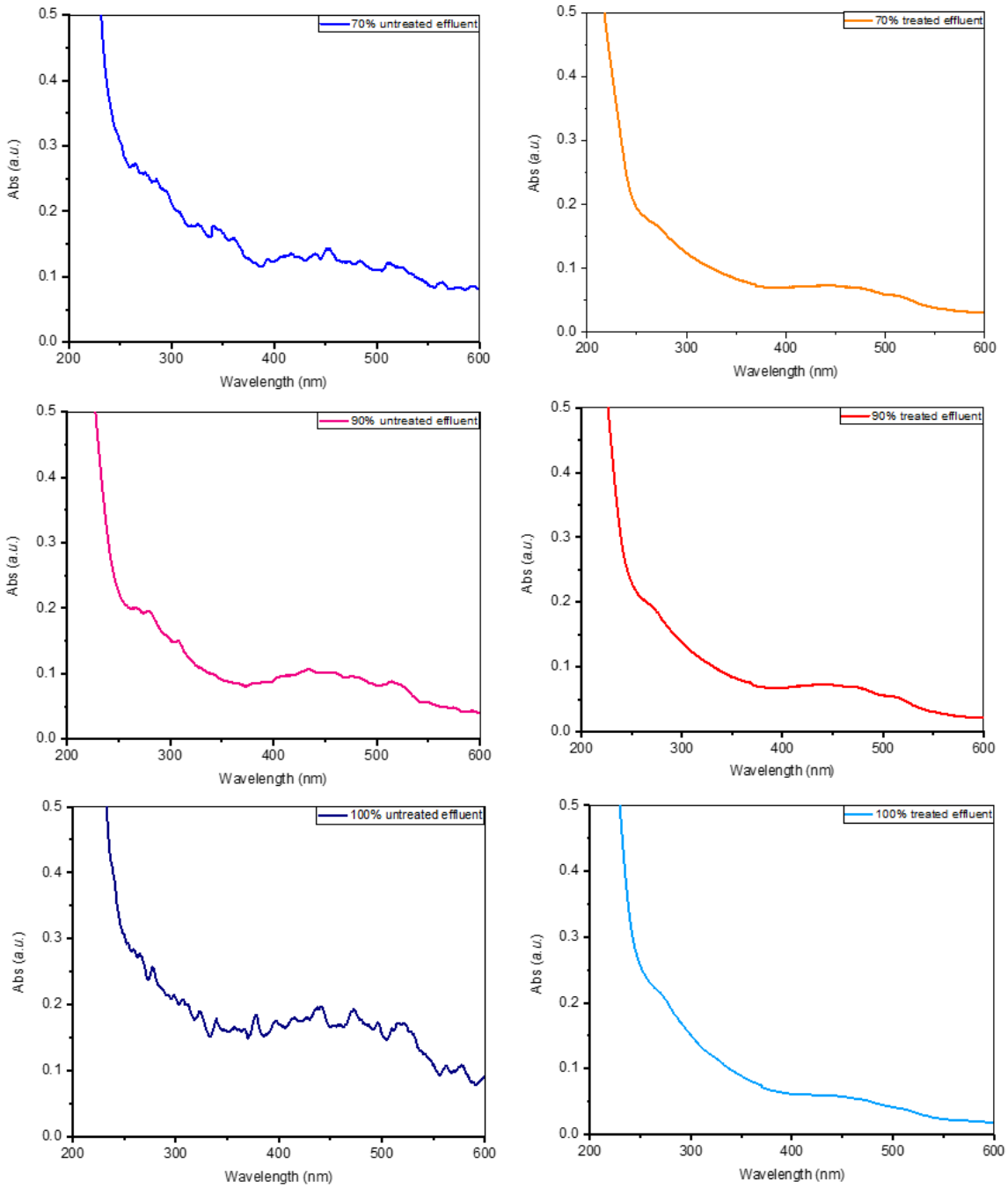

Fig. 9. UV-Vis absorption spectra of different concentrations of treated and untreated food-based effluents

Because the preparation was not demonstrated to contain exclusively purified LiP, the observed activity is referred to as activity of the crude ligninolytic enzyme preparation. The possible contribution of other extracellular oxidative enzymes cannot be excluded. After being heated to 80 °C for two hours, the collected food-processing wastewater was filtered. Absorbance measurements were taken both before and after physical treatment, since this prior procedure can autonomously remove floating or colloidal color-causing material. The reduction seen following physical pretreatment was taken into consideration independently of the reduction seen following enzyme/material therapy. Instead of assuming that all color reduction was due to enzymatic action, the apparent removal ascribed to the enzyme-produced material was assessed in relation to the physically processed effluent.

The treated and untreated food wastewater samples were prepared at concentrations of 30%, 50%, 70%, 90%, and 100% (v/v), with each percentage representing the proportion of food wastewater in the final sample; therefore, 100% refers to undiluted wastewater. Figure 9 shows the spectral characteristics of the food effluent samples, with the 30% and 50% preparations displaying broad absorbance bands across the visible region, likely due to the presence of colloidal particles, organic matter, and mixed colorants (Chen *et al.* 2019). Following treatment, a noticeable reduction in absorbance intensity was observed across the tested concentrations, with the 30% effluent showing the greatest increase in transparency (Aragaw and Bogale 2021). The absence of substantial shifts in the major absorption bands suggests that the observed changes were mainly associated with destabilization and aggregation of colloidal and organic components rather than complete oxidative destruction of the chromophoric groups (Kulasooriya *et al.* 2020). Similar findings have been reported for industrial effluents, where treatment reduced turbidity and color while persistent dye structures were not completely mineralized (Miyah *et al.* 2020).

Apparent Color Removal from Food-Processing Effluent by Enzymes

Under the investigated conditions, UV-Vis absorbance decreased when the food processing wastewater was treated. Although this decline suggests a decrease in optical color intensity, it does not prove that the color-causing chemicals had completely degraded or mineralized. A few concurrent processes, such as adsorption onto charcoal, crystallization or removal of dispersed material, oxidation mediated by hydrogen peroxide, and enzymatic conversion by the crude ligninolytic preparation, could be responsible for the observed reduction. As a result, apparent color reduction is the main interpretation of the data. To demonstrate mineralization or identify transformation products, additional analyzes like COD, TOC, HPLC, or LC-MS would be needed.

Crude LiP was used to study the enzymatic breakdown of dye found in food processing effluent. The spectrophotometric results are shown in Fig. 10. The graphical data show that the effluent samples' LiP activity significantly increased.

A specific dilution of the studied enzyme showed the highest LiP activity, suggesting that the ideal concentration of the enzyme is necessary to achieve effective catalytic oxidation of dye molecules (Dube *et al*. 2024). While inadequate enzyme loading limits the availability of catalytic active sites, which lowers breakdown efficiency, excessive enzyme concentrations can cause enzyme aggregation or substrate inhibition. By using hydrogen peroxide as an electron acceptor to start one-electron oxidation events, LiP's catalytic oxidative mechanism is responsible for the observed decrease in dye absorption (Kumar *et al*. 2024). LiP has a high redox potential and may oxidize a wide range of aromatic chemicals, both phenolic and non-phenolic, that are commonly found in

commercial dyes. The LiP transforms hydrogen peroxide into reactive intermediates (Compounds I and II) throughout the catalytic cycle (Fu *et al*. 2025). These intermediates then oxidize dye molecules by abstracting electrons.

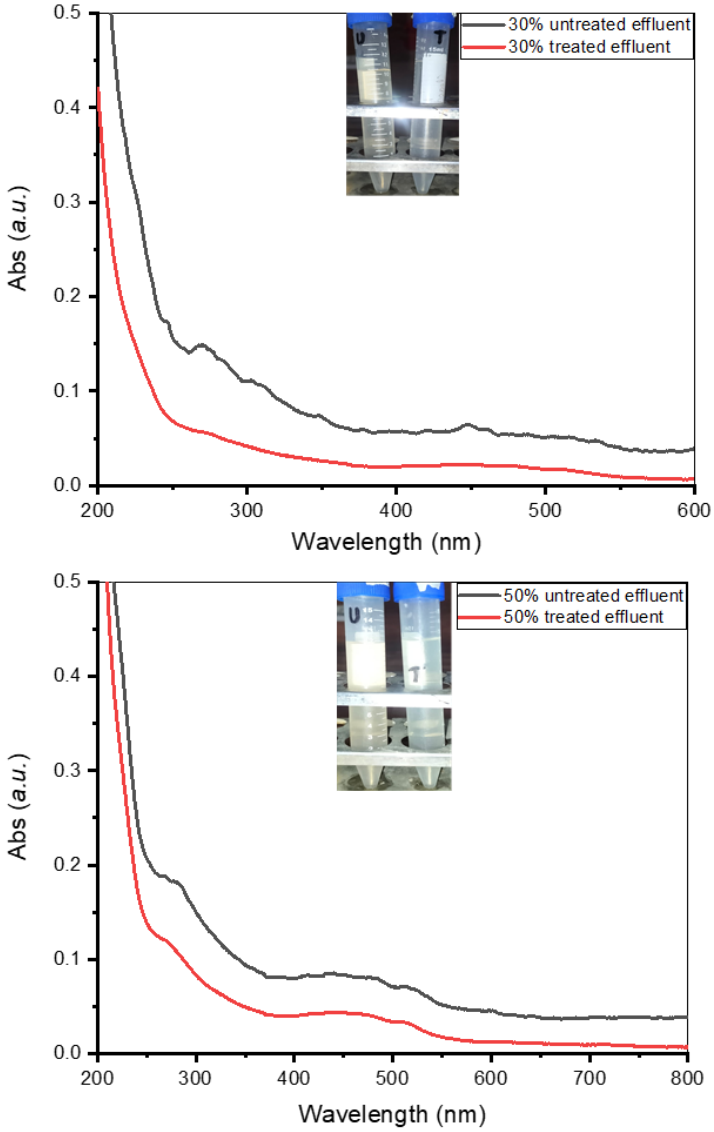

Fig. 10. UV-Vis absorption spectra of 30% and 50% dilutions of treated and untreated food-based effluents

Complex aromatic compounds are cleaved into smaller, less colorful intermediates because of this process, which also destabilizes the conjugated chromophoric complexes responsible for coloration (Rath *et al*. 2025). Recent research has revealed similar findings, showing that ligninolytic enzymes are highly effective at breaking down heterocyclic ring patterns and lowering the toxicity of colorful industrial effluents. As a result, the study's findings demonstrate lignin peroxidase's efficacy as a strong biological catalyst for the decomposition of wastewater from the food industry and highlight its potential use in ecologically friendly wastewater treatment systems (Savinova and Fedorova 2024).

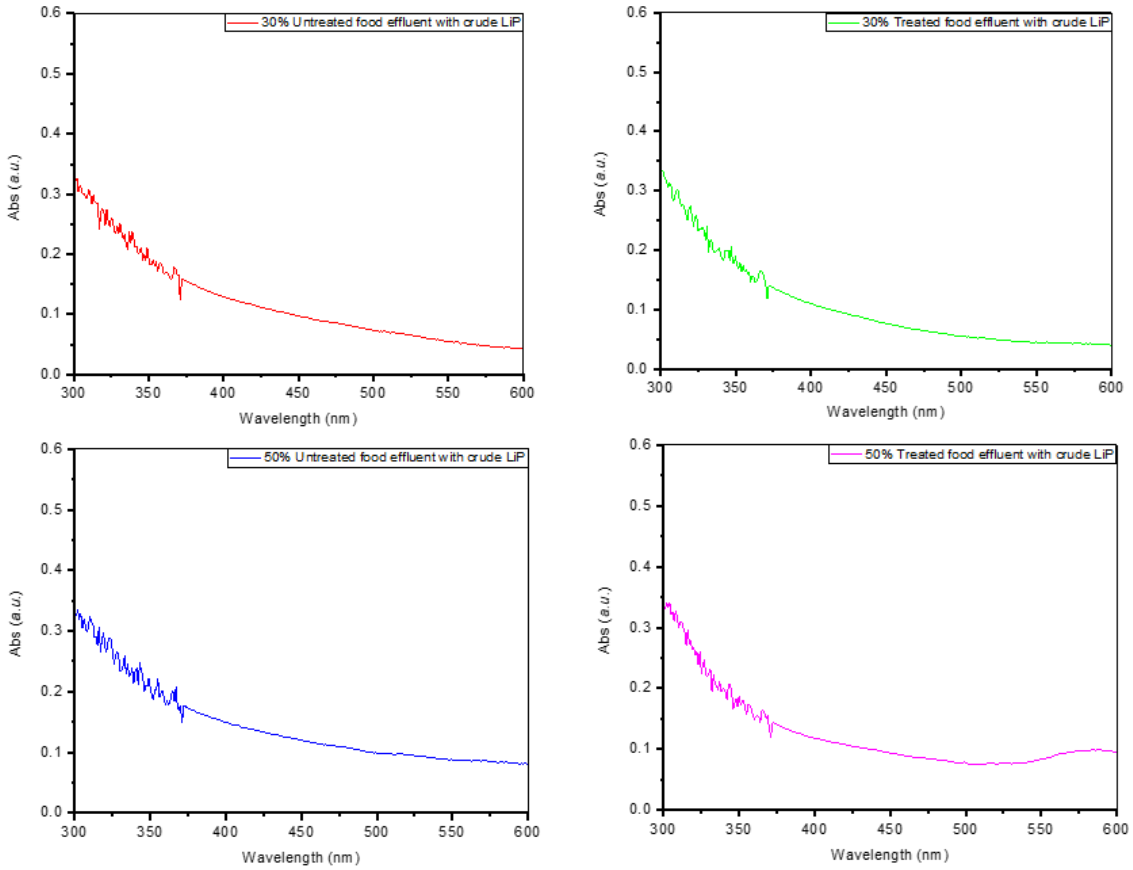

Fig. 11. UV-Vis absorption spectra of 30% and 50% dilutions of treated and untreated food-based effluents treated with LiP for dye degradation

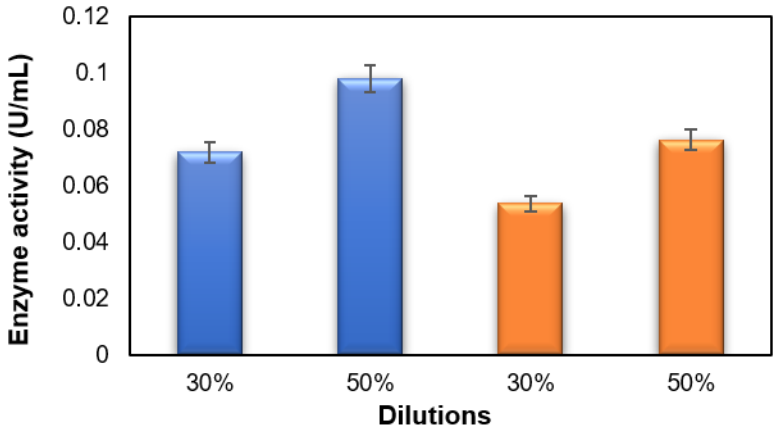

Fig. 12. Crude LiP activity for the degradation of untreated (blue) and treated (orange) food effluent in different dilutions

FUTURE PERSPECTIVES

1. Future studies could further compare the kinetic behavior of free and immobilized enzyme preparations under the same experimental conditions. Determining the Michaelis constant (K_m), maximum reaction velocity (V_{max}), and catalytic efficiency

would provide a clearer understanding of whether immobilization influences substrate affinity and overall enzyme performance.

2. When evaluating the current findings, a number of limitations should be considered. First, the particular chemical identification of the colorants was not independently determined, and industrial effluent contained a complicated mixture of organic and color-causing substances. Second, adsorption, precipitation, oxidation by chemicals, and enzymatic activation cannot all be distinguished by a decrease in UV-Vis absorbance alone. Third, before operational reusability can be determined, quantitative evaluation of enzyme loading, enzyme leaching, long-term stability, regeneration, and numerous treatment cycles is necessary.
3. In future research, comprehensive effluent assessment, standard adsorption controls, enzyme-specific controls, COD/TOC measurements, chromatographic identification of conventional oxidation products, toxicity evaluation, BET surface-area analysis, enzyme-loading measurements, and repeated treatment cycles should all be included. These studies would offer a more solid foundation for evaluating the charcoal-supported ligninolytic enzyme system's treatment capacity, mechanism, cost, and potential for scaling up.

CONCLUSIONS

In order to improve the breakdown of dyes found in food effluents, charcoal particles were successfully produced and modified for the stabilization of lignin peroxidase isolated from *Trametes versicolor*.

1. A stable biocatalytic system was produced by successfully cross-linking the enzyme onto carbodiimide-activated charcoal particles. In this study, to guarantee the highest recovery and activity of lignin peroxidase (LiP), the crude mushroom extract formulation was improved.
2. The effectiveness of dye removal was compared using free and bound or cross-linked LiP samples. The findings showed that, in comparison to its free equivalent, immobilized LiP showed noticeably improved stability.
3. Better substrate availability and catalytic engagement were made possible by the charcoal NPs' large surface area and ideal condition for enzyme attachment.
4. In addition to immobilizing enzymes, charcoal NPs also aided in adsorption-assisted degradation, which improved the removal process as a whole.
5. Optimization tests showed that the breakdown rate was strongly affected by certain enzyme and nanoparticle concentrations.

FUNDING

The authors express their gratitude to Princess Nourah bint Abdulrahman University Researchers Supporting Project number PNURSP2026R214, Princess Nourah bint Abdulrahman University, Riyadh, Saudi Arabia. This work was supported by the

Deanship of Scientific Research, Vice Presidency for Graduate Studies and Scientific Research, King Faisal University, Saudi Arabia [Grant No. KFU264849]

Competing Interests

The authors declare that there are no conflicts of interest.

Availability of Data and Material

All the data generated in this research work has been included in this manuscript.

REFERENCES CITED

Adamian, Y., Lonappan, L., Alokpa, K., Agathos, S. N., and Cabana, H. (2021). "Recent developments in the immobilization of Laccase on carbonaceous supports for Environmental applications – A critical review," *Front. Bioeng. Biotechnol.* 9, article 778239. https://doi.org/10.3389/fbioe.2021.778239

Akbari, B., Tavandashti, M. P., and Zandrahimi, M. (2011). "Particle size characterization of nanoparticles – A practical approach," *Ira. J. Mat. Sci. Engin.* 8(2), 48-56, http://ijmse.iust.ac.ir/files/site1/user_files_4qu804/ijmse-A-10-3-149-c629680.pdf

Alkrad, J. A., Mrestani, Y., Stroehl, D., Wartewig, S., and Neubert, R. (2003). "Characterization of enzymatically digested hyaluronic acid using NMR, Raman, IR, and UV-Vis spectroscopies," *J. Pharm. Biomed. Anal.* 31(3), 545-550. https://doi.org/10.1016/s0731-7085(02)00682-9

Ameen, F., Karimi-Maleh, H., Darabi, R., Akin, M., Ayati, A., Ayyildiz, S., Bekmezci, M., Bayat, R., and Sen, F. (2023). "Synthesis and characterization of activated carbon supported bimetallic Pd based nanoparticles and their sensor and antibacterial investigation," *Environ. Res.* 221, article 115287. https://doi.org/10.1016/j.envres.2023.115287

Ankush, K., Pugazhenthi, G., Mohit, K., and Vasanth, D. (2022). "Experimental study on fabrication, biocompatibility and mechanical characterization of polyhydroxy-butyrate-ball clay bionanocomposites for bone tissue engineering," *Int. J. Biol. Macromol.* 209(Pt B), 1995-2008. https://doi.org/10.1016/j.ijbiomac.2022.04.178

Aragaw, T. A., and Bogale, F. M. (2021). "Biomass-based adsorbents for removal of dyes from wastewater: A review," *Front. Environ. Sci.* 9, article 764958. https://doi.org/10.3389/fenvs.2021.764958

Borang, N., Dutta, A., and Yadav, M. (2025). "Structural insights, bio-catalytic characteristics, and application prospects of lignin peroxidase for sustainable biotechnology – A critical review of recent progress and future directions," *Trends Sci.* 22(6), article 9716. https://doi.org/10.48048/tis.2025.9716

Boukoussa, B., Cherdouane, K. R., Zegai, R., Mokhtar, A., Hachemaoui, M., Issam, I., Iqbal, J., Patole, S. P., Zeggai, F. Z., Hamacha, R., and Abboud, M. (2023). "Preparation of activated carbon-metal nanoparticle composite materials for the catalytic reduction of organic pollutants," *Surf. Interfac.* 44, article 103622. https://doi.org/10.1016/j.surfin.2023.103622

Cao, D., Zhu, X., Zhang, J., and Wang, M. (2023). "A combined strategy to enhance phytosterols biotransformation to 22-hydroxy-23, 24-bisnorchol-4-ene-3-one by

Mycobacterium neoaurum," *Process Biochem.* 128, 94-97. https://doi.org/10.1016/j.procbio.2023.02.019

Chen, X., Zhou, J., Zhang, T., and Ding, L. (2019). "Enhanced degradation of tetracycline hydrochloride using photocatalysis and sulfate radical-based oxidation processes by Co/BiVO4 composites," *J. Water Process Eng.* 32, article 100918. https://doi.org/10.1016/j.jwpe.2019.100918

Choudhary, F., Mudgal, P., Parvez, A., Sharma, P., and Farooqi, H. (2024). "A review on synthesis, properties and prospective applications of carbon nanomaterials," *Nano Struct. Nano Objects* 38, article 101186. https://doi.org/10.1016/j.nanoso.2024.101186

Collins, S. E., Lassalle, V., and Ferreira, M. L. (2011). "FTIR-ATR characterization of free *Rhizomucor meihei* lipase (RML), Lipozyme RM IM and chitosan-immobilized RML," *J. Mol. Cat. B Enzymatic* 72(3-4), 220-228. https://doi.org/10.1016/j.molcatb.2011.06.009

Costa, F. C. R., Brito, F. S. L., De Grandi, M. J. R., and Daniel., J. F. S. (2025). "White Rot Fungi for biodegradation of dyes: Potential for industrial uses – A review," *J. Braz. Chem. Soc.* 36(3), article 20250024. https://doi.org/10.21577/0103-5053.20250024

Cross, S. N., Korpany, K. V., Zakaria, H., and Blum, A. S. (2025). "Cross-reactivities in conjugation reactions involving iron oxide nanoparticles," *Beilstein J. Nanotechnol.* 16, 1504-1521. https://doi.org/10.3762/bjnano.16.106

Danmallam, U. N., Adeleke, A. A, Zango, Z .U., Bakar, N. H. H. A., Gimba, A. S. B., Rasheed, H. A., and Baffa, A. A. (2025). "Adsorptive removal of phenanthrene and naphthalene from wastewater using coal derived carbon nanoparticles with kinetic and thermodynamic evaluation," *Sci. Rep.* 15(1), article 39118. https://doi.org/10.1038/s41598-025-27116-4

Ding, G., Qin, G., Ying, W., Wang, P., Yang, Y., Tang, C., Liu, Q., Li, M., Huang, K., and Chen, S. (2024). "Nano-silver-loaded activated carbon material derived from waste rice noodles: Adsorption and antibacterial performance," *Nanomater.* 14(22), article 1857. https://doi.org/10.3390/nano14221857

Dogan, Y., Oziç, C., Ertaş, E., Baran, A., Rosic, G., Selakovic, D. and Eftekhari, A. (2024). "Activated carbon-coated iron oxide magnetic nanocomposite loaded with morin hydrate for drug-delivery applications," *Front. Chem.* 12, article 1477724. https://doi.org/10.3389/fchem.2024.1477724

Dube, S. L., Osunsanmi, F. O., Ikhane, A. O., Mosa, R. A., and Opoku, A. R. (2024). "Biodegradation and detoxification of some dyes by crude lignin peroxidase complex produced by *Escherichia coli* and *Pseudomonas aeruginosa*," *Appl. Sci.* 14(17), article 8012. https://doi.org/10.3390/app14178012

Fu, N., Liu, R., Zhou, Y., Li, B., Yuan, Y., and Liu, Z. (2025). "Technological advances in ligninolytic enzymes for the biological valorization of lignin," *Green Chem.* 27(16), 4016-4039. https://doi.org/10.1039/d4gc05724d

Giap, V. D., Nghi, D. H., Cuong, L. H. and Quynh, D. T. (2022). "Lignin peroxidase from the white-rot fungus *Lentinus squarrosulus* MPN12 and its application in the biodegradation of synthetic dyes and lignin," *BioResources* 17(3), 4480-4498. https://doi.org/10.15376/biores.17.3.4480-4498

Grisolia, A., De Santo, M., Curcio, M., Cavallaro, P.A., Morelli, C. Leggio, A., and Pasqua, L. (2024). "Engineered mesoporous silica-based nanoparticles:

Characterization of surface properties," *Mater.* 17(13), article 3352. https://doi.org/10.3390/ma17133352

Gye, H., Baek, H., Han, S., Kwon, H., Nguyen, T. V. T., Pham, L. T. M., Kang, S., Nho, Y. H., Lee, D. W., and Kim, Y. H. (2023). "Recombinant lignin peroxidase with superior thermal stability and melanin decolorization efficiency in a typical human skin-mimicking environment," *Biomacromolecules* 24(6), 2633-2642. https://doi.org/10.1021/acs.biomac.3c00123

Jing, H., Bardakci, F., Akgol, S., Kusat, K., Adnan, M., Alam, M., Gupta, R., Sahreen, S., Chen, Y., Gopinath, S., and Sasidharan, S. (2023). "Green carbon dots: Synthesis, characterization, properties and biomedical applications," *J. Funct. Biomater.* 14(1), article 27. https://doi.org/10.3390/jfb14010027

Joudeh, N., and Linke, D. (2022). "Nanoparticle classification, physicochemical properties, characterization, and applications: A comprehensive review for biologists," *J. Nanobiotechnol.* 20(1), article 262. https://doi.org/10.1186/s12951-022-01477-8

Kamal, A., Saba, M., Ullah, K., Almutairi, S. M., AlMunqedhi, B. M., and Gawwad, M. R. (2023). "Mycosynthesis, characterization of zinc oxide nanoparticles, and its assessment in various biological activities," *Crystals* 13(2), article 171. https://doi.org/10.3390/cryst13020171

Kirubakaran, D., Wahid, J. B. A., Karmegam, N., Jeevika, R., Sellapillai, L., Rajkumar, M., and SenthilKumar, K. J. (2025). "A Comprehensive review on the green synthesis of nanoparticles: Advancements in biomedical and environmental applications," *J. Biomed. Mater. Res.* 4(1), 388-413. https://doi.org/10.1007/s44174-025-00295-4

Kouassi, G. K., Irudayaraj, J., and McCarty, G. (2005). "Activity of glucose oxidase functionalized onto magnetic nanoparticles," *BioMagn. Res. Technol.* 3(1), 1. https://doi.org/10.1186/1477-044x-3-1

Kousar, K., Naseer, F., Abduh, M. S., Kakar, S., Gul, R., Anjum, S., and Ahmad, T. (2023). "Green synthesis of hyaluronic acid coated, thiolated chitosan nanoparticles for CD44 targeted delivery and sustained release of Cisplatin in cervical carcinoma," *Front. Pharmacol.* 13, article 1073004. https://doi.org/10.3389/fphar.2022.1073004

Kulasooriya, T. P. K., Priyantha, N., and Navaratne, A. N. (2020). "Removal of textile dyes from industrial effluents using burnt brick pieces: Adsorption isotherms, kinetics and desorption," *Discov. Appl. Sci.* 2(11). https://doi.org/10.1007/s42452-020-03533-0

Kumar, V., Pallavi, P., Sen, S. K. and Raut, S. (2024). "Harnessing the potential of white rot fungi and ligninolytic enzymes for efficient textile dye degradation: A comprehensive review," *Water Environ.t Res.* 96(1), article e10959. https://doi.org/10.1002/wer.10959

Lin, P., Lin, S., Wang, P. C., and Sridhar, R. (2013). "Techniques for physicochemical characterization of nanomaterials," *Biotechnol. Adv.* 32(4), 711-726. https://doi.org/10.1016/j.biotechadv.2013.11.006

Ma, X., Pronay, T. S., Gao, B., and Zhao, J. (2025). "Nano-engineered enzyme immobilization: toward biomedical, orthopedic, and biofuel applications," *ACS Omega* 10(32), 35434-35450. https://doi.org/10.1021/acsomega.5c05589

Manimaran, M., Norizan, M. N., Kassim, M. H. M., Adam, M. R., Abdullah, N., and Norrrahim, M. N. F. (2025). "Critical review on the stability and thermal conductivity of water-based hybrid nanofluids for heat transfer applications," *RSC Adv.* 15(18), 14088-14125. https://doi.org/10.1039/d5ra00844a

Mathur, P., and Pillai, S. (2025). "Fungi-mediated nanomaterials: Advances, synthesis pathways, and limitations," *Fungal Biol. Rev.* 54, article 100445. https://doi.org/10.1016/j.fbr.2025.100445

McNeil, S. E. (2018). "Characterization of nanoparticles intended for drug delivery," *Meth. Mol. Biol*. 162, 65-71. https://doi.org/10.1007/978-1-4939-7352-1

Miyah, Y., Lahrichi, A., Kachkoul, R., Mouhri, G. E., Idrissi, M., Iaich, S., and Zerrouq, F. (2020). "Multi-parametric filtration effect of the dyes mixture removal with the low cost materials," *Arab J. Basic Appl. Sci.* 27(1), 248-258. https://doi.org/10.1080/25765299.2020.1776008

Mohammed, A. A., Merrild, N. G., Li, S., Pinna, A., and Jones, J. R. (2022). "Double-network hydrogels reinforced with covalently bonded silica nanoparticles via 1-ethyl-3-(3-dimethylaminopropyl) carbodiimide chemistry," *ACS Omega* 7(48), 43904-43914. https://doi.org/10.1021/acsomega.2c05169

Mourdikoudis, S., Pallares, R. M., and Thanh., N. T. K. (2018). "Characterization techniques for nanoparticles: Comparison and complementarity upon studying nanoparticle properties," *Nanoscale* 10(27), 12871-12934. https://doi.org/10.1039/c8nr02278j

Negi, B. B., Umesh, N., and Das, C. (2025). "Understanding the role of lignin peroxidase (LiP) from *Phanerochaete chrysosporium* for refinery wastewater remediation: Insights from molecular docking and simulation," *Int. J. Biol. Macromol.* 330(Pt 2), article 148044. https://doi.org/10.1016/j.ijbiomac.2025.148044

Onley, J. R., Gupta, K., De Raad, M., Bowen, B. P., Tan, S., Yoder, S., Sale, K. L., Singh, A. K., Simmons, B. A., Northen, T. R., and Deng, K. (2025). "Enzymatic cleavage of model lignin dimers depends on pH, enzyme, and bond type," *Sci. Rep.* 15(1), article 10296. https://doi.org/10.1038/s41598-025-88571-7

Panda, J., Nongbet, A., Avula, S. K., Nayak, D., Rustagi, S., Panda, B. P., and Mohanta, Y. K. (2025). "Macro-fungi mediated nanoparticles for sustainable agriculture: Recent advancement and future strategies," *Discov. Sustain.* 6(1). https://doi.org/10.1007/s43621-025-01219-4

Park, J. Y., Han, S., Kim, D., Nguyen, T. V. T., Nam, Y., Kim, S. M., Chang, R., and Kim, Y. H. (2024). "Enhancing the thermostability of lignin peroxidase: Heme as a keystone cofactor driving stability changes in heme enzymes," *Heliyon* 10(17), article e37235. https://doi.org/10.1016/j.heliyon.2024.e37235

Ragib, A. A., Amin, A. A., Alanazi, Y. M., Kormoker, T., Uddin, M., Siddique, M. a. B., and Barai, H. R. (2023). "Multifunctional carbon dots in nanomaterial surface modification: A descriptive review," *Carbon Res.* 2(1). https://doi.org/10.1007/s44246-023-00069-x

Rath, S., Mohapatra, R. K., Mohapatra, S., Panda, A. K., and Thatoi, H. (2025). "Degradation of cationic dyes and alkali lignin using DyP-producing *Bacillus cereus* SDP6 isolated from similipal biosphere reserve soil," *Sci. Rep.* 15(1), article 31347. https://doi.org/10.1038/s41598-025-16278-w

Sajjad, K., Kainaat, H., Ehsan, A., Sukmawati, D., Anvar, A. H., Shakir, H. A., Khan, M., Franco, M., and Irfan, M. (2025). "Lignases: Current status, production, optimization, applications and future prospects," *J. Umm Al-Qura Univ. Appl. Sci*. https://doi.org/10.1007/s43994-025-00287-6

Savinova, O. S., and Fedorova, T. V. (2024). "Peroxidase of *Trametes hirsuta* LE-BIN 072: Purification, characteristics, and application for dye decolorization," *Appl. Biochem. Microbiol.* 60(6), 1209-1222. https://doi.org/10.1134/s0003683824605730

Sen, T. K. (2023). "Application of synthesized biomass bamboo charcoal-iron oxide BC/Fe nanocomposite adsorbents in the removal of cationic methylene blue dye contaminants from wastewater by adsorption," *Sustainability* 15(11), article 8841. https://doi.org/10.3390/su15118841

Shahzadi, S., Fatima, S., Ain, Q. U., Shafiq, Z., and Janjua, M. R. S. A. (2025). "A review on green synthesis of silver nanoparticles (SNPs) using plant extracts: A multifaceted approach in photocatalysis, environmental remediation, and biomedicine," *RSC Adv.* 15(5), 3858-3903. https://doi.org/10.1039/d4ra07519f

Sharpe, E., Farragher-Gnadt, A.P., Igbanugo, M., Huber, T., Michelotti, J. C., Milenkowic, A., Ludlam, S., Walker, M., Hanes, D., Bradley, R., and Bou-Abdallah, F. (2021). "Comparison of antioxidant activity and extraction techniques for commercially and laboratory prepared extracts from six mushroom species," *J. Agr. Food Res.* 4, 100-130. https://doi.org/10.1016/j.jafr.2021.100130

Singh, A. K., Katari, S. K., Umamaheswari, A., and Raj, A. (2021). "*In silico* exploration of lignin peroxidase for unraveling the degradation mechanism employing lignin model compounds," *RSC Adv.* 11(24), 14632-14653. https://doi.org/10.1039/d0ra10840e

Singh, K., Bharose, R., Verma, S. K., and Singh, V. K. (2012). "Potential of powdered activated mustard cake for decolorising raw sugar," *J. Sci. Food Agric.* 93(1), 157-165. https://doi.org/10.1002/jsfa.5744

Sitinjak, N. A., Huang, C., Yang, T., Chau, L., and Wang, C. (2025). "Synthesis of carboxymethyl dextran-coated gold nanoparticles as stable and storable optical labels for ultrasensitive plasmonic nanoparticle-linked sorbent assay," *Sensors* 25(23), article 7156. https://doi.org/10.3390/s25237156

Suryadi, H., Judono, J. J., Putri, M. R., Eclessia, A. D., Ulhaq, J. M., Agustina, D. N., and Sumiati, T. (2022). "Bio-delignification of lignocellulose using ligninolytic enzymes from white-rot fungi," *Heliyon* 8(2), e08865. https://doi.org/10.1016/j.heliyon.2022.e08865

Talam, S., Karumuri, S. R., and Gunnam, N. (2012). "Synthesis, characterization, and spectroscopic properties of ZNO nanoparticles," *ISRN Nanotechnol.* 1-6. https://doi.org/10.5402/2012/372505

Thuan, N. D., Cuong, H. M., Nam, N. H., Huong, N. T. L., and Hong, H. S. (2024). "Morphological analysis of Pd/C nanoparticles using SEM imaging and advanced deep learning," *RSC Adv.* 14(47), 35172-35183. https://doi.org/10.1039/d4ra06113f

Vrsanska, M., Voberkova, S., Langer, V., Palovcikova, D., Moulick, A., Adam, V., and Kopel, P. (2016). "Induction of laccase, lignin peroxidase and manganese peroxidase activities in white-rot fungi using copper complexes," *Molecules* 21(11), article 1553. https://doi.org/10.3390/molecules21111553

Wadhwa, P., Sharma, S., Sahu, S., Sharma, A., and Kumar, D. (2022). "A review of nanoparticles characterization techniques," *Curr. Nanomater.* 7(3), 202-214. https://doi.org/10.2174/2405461507666220405113715

Wang, Q., Lv, K., Song, J., Li, M., Ouyang, X., Liu, C., Gong, S., Wang, J., Li, J., and Zhang, Z. (2025). "The dose-dependent effect of carbon quantum dots as a photosynthesis enhancer on soybean plant growth," *Nanomaterials* 15(20), article 1603. https://doi.org/10.3390/nano15201603

Zhang, Y., Zheng, Y., Yang, Y., Huang, J., Zimmerman, A. R., Chen, H., Hu, X., and Gao, B. (2021). "Mechanisms and adsorption capacities of hydrogen peroxide modified ball milled biochar for the removal of methylene blue from aqueous solutions," *Bioresour. Technol.* 337, article 125432. https://doi.org/10.1016/j.biortech.2021.125432

Zhao, C., Ma, X., Duan, X., Guo, Q., Niu, S., Zhou, W., Cao, Y., and Yuan, C. (2023). "Synthesis of novel adsorbent S-SiO_2-Fe_3O_4 based on strong bonding of S-O-Se for selenium removal in water," *J. Environ. Chem. Eng.* 11(3), article 109782. https://doi.org/10.1016/j.jece.2023.109782

Article submitted: April 6, 2026; Peer review completed: August 15, 2026; Revised version received: September 3, 2026; Accepted: September 4, 2026; Published: September 22, 2026.
DOI: 10.15376/biores.21.4.10958-10983